JACS
JOURNAL OF THE AMERICAN CHEMICAL SOCIETY

Article

pubs.acs.org/JACS

Anatomy of an Oligourea Six-Helix Bundle

Caterina M. Lombardo,[†,‡,∇] Gavin W. Collie,[†,‡,∇,¶] Karolina Pulka-Ziach,[†,‡,○] Frederic Rosu,[§] Valerie Gabelica,[∥,⊥] Cameron D. Mackereth,[∥,⊥] and Gilles Guichard*[,†,‡]

[†]Université de Bordeaux, CBMN, UMR 5248, Institut Européen de Chimie et Biologie, 2 rue Robert Escarpit, 33607 Pessac, France
[‡]CNRS, CBMN, UMR 5248, 33600, Pessac, France
[§]CNRS, UMS3033/US001, Institut Européen de Chimie et Biologie, 33607 Pessac, France
[∥]Université de Bordeaux, Institut Européen de Chimie et Biologie, 2 rue Robert Escarpit, 33607 Pessac, France
[⊥]Inserm, U1212, ARNA Laboratory, 146 rue Léo Saignat, 33076 Bordeaux, France

Supporting Information

ABSTRACT: Non-natural synthetic oligomers that adopt well-defined secondary structures (i.e., foldamers) represent appealing components for the fabrication of bioinspired self-assembled architectures at the nanometer scale. Recently, peptidomimetic N,N′-linked oligourea helices have been designed *de novo* with the ability to fold into discrete helix bundles in aqueous conditions. In order to gain better insight into the determinants of oligourea helix bundle formation, we have investigated the sequence-to-structure relationship of an 11-mer oligourea previously shown to assemble into a six-helix bundle. Using circular dichroism, NMR spectroscopy, native mass-spectrometry and X-ray crystallography, we studied how bundle formation was affected by systematic replacement of the hydrophobic surface of the oligourea helix with either polar or different hydrophobic side chains. The molecular information gathered here has revealed several key requirements for foldamer bundle formation in aqueous conditions, and provides valuable insight toward the development of foldamer quaternary assemblies with improved (bio)physical properties and divergent topologies.

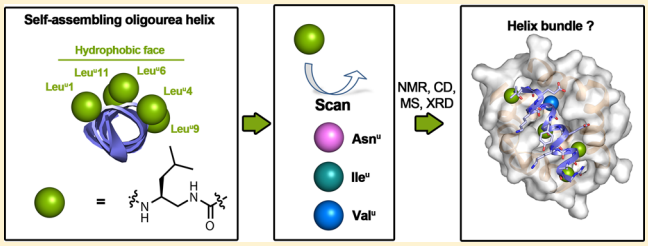

INTRODUCTION

Peptide α-helices packed into coiled coil arrangements have generated a long-standing interest in protein study and design, in part because they represent a highly prevalent motif among tertiary and quaternary structures of proteins[1] but also because they provide unique and versatile building blocks for the creation of artificial biomolecular systems.[2,3] Coiled coils (also referred to as helix bundles) commonly observed in proteins consist of two to four (or more) amphiphilic α-helices, which associate through the hydrophobic effect, the driving force of helix bundle formation.[1,4−6] The interfaces between helices of a coiled coil are predominantly composed of hydrophobic amino acid residues (i.e., Leu, Ile, Val) packed into "knobs-into-holes" (KIH) arrangements. These hydrophobic residues are typically positioned at the *a* and *d* positions of the α-helix heptad repeat (labeled *abcdefg*). The spatially flanking *e* and *g* positions are often occupied by amino acids with charged side chains, which, through ionic interactions, contribute to the overall topology (e.g., the orientation of helices) and stability of the coiled coil, as well as providing a pH-dependence to the assemblies.[3,7,8] Despite their apparent simplicity, coiled coils are extremely diverse[4,6] and are highly sensitive to sequence changes. Combined experimental and computational efforts have contributed to unveiling the origins of both the specificity and stability of coiled coils (such as the complementarity of the *a* and *d* positions and the role of buried polar groups),[4,5,9] permitting the design of new coiled coil topologies[10−13] and unprecedented assemblies at the nanometer scale[14−18] for possible applications in material science and synthetic biology.[2,3,19]

More recently, the folding and assembly principles of coiled coils have been applied to artificial backbones (i.e., foldamers[20−22]), in an attempt to create increasingly diverse higher-order structures with oligomerization states and shapes beyond those found in nature.[23,24] A handful of high resolution structural studies of self-assembled foldamers in aqueous conditions have been reported, creating new opportunities in foldamer design.[25−33] Foldamer helix bundles of various stoichiometries have been characterized in the crystal state, including β^3-peptide octameric helix bundles,[26−28] tetrameric bundles formed from α,β-peptide hybrid helices,[29−31] and a hexameric bundle formed from N,N′-linked oligoureas with proteinogenic side chains.[32,33] In the case of oligoureas, alternative aqueous topologies (i.e., superhelical channels with tunable diameters) can also be formed by changing the proportion and distribution of hydrophilic and hydrophobic side chains at the helical surface. Although these structures are

Received: May 17, 2016
Published: July 19, 2016

DOI: 10.1021/jacs.6b05063
J. Am. Chem. Soc. 2016, 138, 10522−10530

illuminating, there is still much to learn about sequence-to-structure relationships as a means to improve *de novo* design of foldamers with the ability to self-assemble into defined nanostructures in aqueous conditions and possibly develop new functional materials.[24,34] Here, we are focusing on **H1**, an 11-mer oligourea previously found to fold into a six-helix bundle in aqueous conditions (Figure 1A).

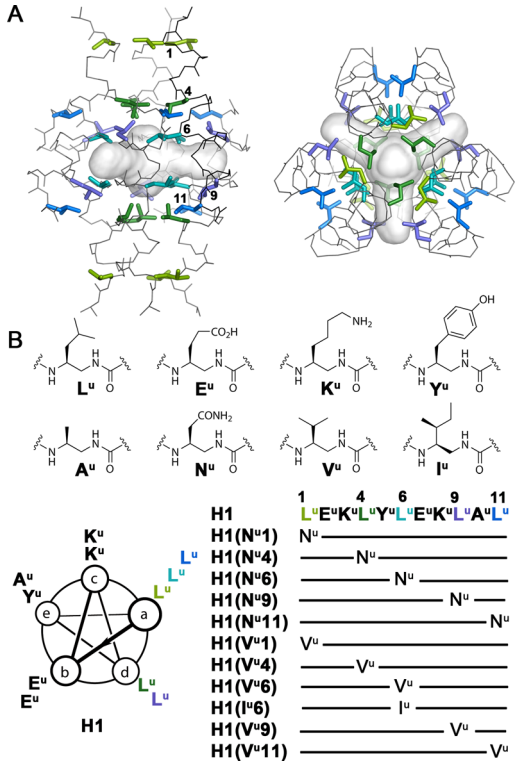

Figure 1. (A) Crystal structure of a six-helix bundle formed from **H1**.[32] The six isobutyl side chains in the sequence of **H1** are colored differently to highlight their respective location in the bundle. The resulting internal cavity that is formed upon self-assembly is shown as a white surface representation. (B) Sequences of **H1** and of the 11 monosubstituted analogues that have been prepared and evaluated in the present work. A one-letter-code similar to that used for peptides with superscript "u" has been used systematically for urea residues in the sequence (see corresponding formulas).

By analogy to coiled-coil-forming α-peptides, the sequence of **H1** was designed to contain a hydrophobic face formed by leucine-type urea residues (L^u) at the two contiguous *a* and *d* positions of the helical pentad repeat (denoted *abcde* by analogy to the peptide heptad repeat in coiled coils) and flanked by glutamate-type (E^u) and lysine-type (K^u) residues at the *b* and *c* positions, respectively. The 1.25 Å crystal structure of **H1** (Figure 1A) revealed a helix bundle formed from the assembly of six well-defined canonical oligourea helices, with a hydrophobic core and a charged, hydrated exterior (referred to hereafter as the **H1**-bundle) (Figure 1A).[32] As anticipated, all L^u side chains point inward (i.e., away from the solvent), with the majority of them engaged in KIH-type or "ridges-into-grooves"[35] interactions, consistent with the hydrophobic effect playing a key role in the folding and assembly of the **H1**-bundle. It is also apparent from the X-ray crystal structure of the **H1**-bundle (Figure 1A) that, due to the presence of a large isolated cavity (with a volume of ca. 500 $Å^3$), the hydrophobic interior of this bundle differs significantly from those of thermally stable peptide coiled coils and a related β^3-peptide octameric bundle.[28]

In the work described here, we aimed to delineate the role of the L^u residues of the **H1** sequence in bundle formation, as a means to (1) understand essential criteria for oligourea helix-bundle assembly, (2) modify the physical properties of the **H1** six-helix bundle, and (3) evaluate potentially exploitable features of the **H1**-bundle, particularly concerning the internal cavity. Each of the five L^u residues of the **H1** sequence were substituted with either hydrophobic (V^u or I^u) or hydrophilic (N^u) urea residues, with the effects of these mutations on the self-assembly process studied by circular dichroism, native mass spectrometry (ESI-MS), high-field NMR spectroscopy and X-ray crystallography. Our findings reveal that replacement of the L^u residues of **H1** with hydrophilic N^u residues invariably abolishes the formation of detectable discrete self-assemblies, while the effect of hydrophobic substitutions is highly position-dependent and indicates, among other things, that modulation of the size and shape of the hydrophobic cavity of the **H1**-bundle should be feasible. In addition, high-resolution crystallographic studies, including two subangstrom oligourea aqueous crystal structures, provide atomic-scale details of two **H1**-analogue helix bundles and highlight the surprising effects of the aqueous assembly process on foldamer secondary structure.

RESULTS AND DISCUSSION

Polar Residue (N^u) Scanning of the Hydrophobic Face.

Although the *a* and *d* sites of the heptad repeat of peptide coiled coil sequences are generally occupied by hydrophobic residues, polar residues such as Asn and Gln are also frequently found at these positions,[36−38] where they can play a key role in guiding the assembly properties. In the present study, we have evaluated the effect of replacing L^u residues by the corresponding polar asparagine side chain (N^u) in the sequence of **H1**. **H1** contains five L^u residues located at positions 1, 4, 6, 9, and 11 of the sequence (Figure 1), strategically positioned to create a hydrophobic surface to drive specific hydrophobic packing interactions. Previously reported high resolution crystallographic data provided invaluable information concerning the nature of the **H1** bundle assembly. Evidence of the existence of the assembly in solution was supported by NMR analysis and by the observation of specific interhelix NOE cross-peaks. Native electrospray ionization mass spectrometry (ESI-MS), which identified ion $[\mathbf{H1}_6]^{5+}$ as the most populated higher-order species, confirmed the bundle stoichiometry; yet, the modest melting temperature (T_m) value derived from CD-monitored thermal melting experiments (45.9 °C in H_2O) also suggested a certain molten globule character of the assembly, a feature that, if minimized, could improve the physical properties of the **H1** helix-bundle.

In order to investigate the role of the five L^u residues on bundle stability, we performed a full N^u-residue scan of the hydrophobic surface of **H1**. The analogue of **H1** in which the central L^u6 is replaced by N^u, **H1**($\mathbf{N^u6}$), was described previously (referred to therein as **H3**).[32] In contrast to **H1**, there was no clear evidence of stable intermolecular interactions based on NMR studies of this analogue, with ESI-MS showing **H1**($\mathbf{N^u6}$) to display a considerably reduced propensity to self-assemble compared with **H1**. These observations, together with the reduced intensity of the thermal melting profile displayed by **H1**($\mathbf{N^u6}$) compared with **H1**, suggested that the specific self-assembly properties of **H1** were not maintained in

DOI: 10.1021/jacs.6b05063
J. Am. Chem. Soc. 2016, 138, 10522−10530

oligourea **H1**(N^u**6**). Here, **H1** analogues bearing N^u residues at the other L^u positions of **H1**, namely, **H1**(N^u**1**), **H1**(N^u**4**), **H1**(N^u**9**), and **H1**(N^u**11**), were chemically synthesized stepwise on solid support using previously described succinimidyl (2-azido-2-substituted-ethyl) carbamates as building blocks[32,39,40] (see Figure S1 and Supporting Information). Circular dichroism (CD) analysis of the polar mutants revealed all of these molecules to display a helical conformation in water, as indicated by the presence of a molar ellipticity (ME) maximum at 202 nm (Figure S2). Next, interhelix contacts were investigated in solution by NMR in order to ascertain whether higher order assembly was maintained. NOESY experiments were performed for all **H1**-N^u analogues, with the observed sets of NOE cross-peaks compared with those identified for **H1**. Representative NOE cross-peaks detected in **H1** indicative of specific interhelical contacts include those between the aromatic δ or ε protons of Y^u5 side chains in one oligourea molecule and the aliphatic δ1 or δ2 protons of L^u11 side chains in an adjacent oligourea within the hexamer (Figure 2). Significantly, these NOEs are absent in spectra collected for **H1**(N^u**1**), **H1**(N^u**4**), **H1**(N^u**9**), and **H1**(N^u**11**) (as well as for **H1**(N^u**6**)[32]), with no alternative interhelical cross peaks detected, strongly suggesting that these foldamers do not form discrete self-assemblies in aqueous conditions. A further indication of the reduced ability of the N^u-analogues to form stable higher-order structures in water is the absence of NOE signals between the CH_2 protons of K^u side chains (Figure 2). In nonaggregated oligomers, these NOE signals are generally absent, due to fast conformational dynamics of the K^u side chain on an NMR time scale; in contrast these signals can be observed if the molecule is involved in interactions that rigidify the system (e.g., formation of quaternary structures). As expected, such NOE cross-peaks are well-defined for **H1** but could not be detected for **H1**(N^u**1**), **H1**(N^u**4**), **H1**(N^u**9**), or **H1**(N^u**11**). Overall, these experiments indicate that the N^u-mutated oligomers maintain a helical arrangement in aqueous conditions but that, similarly to **H1**(N^u**6**), the specific intermolecular contacts indicative of a well-formed quaternary structure seen in **H1** are not observed. These findings are supported further by comparative analysis of 1D ^{1}H NMR spectra of **H1** versus the mutated oligomers: the 1D ^{1}H signals of **H1** are collectively broader than those of the N^u mutants, consistent with the formation of a larger-sized molecule (Figure S3). Furthermore, the ^{1}H chemical shift values of the side chain methyl protons in **H1** are shifted upfield compared with those of the mutated oligoureas. A similar upfield shift is commonly attributed to a high aliphatic composition within the hydrophobic core of folded proteins and thus supports a stable interior packing of the hydrophobic side chains in hexameric **H1**. The downfield shifts in the N^u mutants are instead indicative of the disassembly of the oligourea bundle.

In addition, ESI-MS spectra determined for the series of oligoureas containing $L^u \rightarrow N^u$ replacements under native conditions revealed extremely low levels of discrete self-assembled species (Figure 2). In most cases, the m/z region above the molecular peak is dominated by background noise (in particular for **H1**(N^u**4**) and **H1**(N^u**9**)), with no clear peak corresponding to specific stoichiometries. MS−MS analysis in the m/z region above 2000, where no sharp peak arises (Figure S4), revealed that the background signal in that region of the mass spectra is actually chemical noise consisting of oligourea monomers (i.e., **H1**(N^u**1**), **H1**(N^u**4**), and **H1**(N^u**9**)), suggesting that these molecules tend to aggregate in solution in a nondiscrete manner. It should be noted that in the case of **H1**(N^u**6**) and **H1**(N^u**11**), it was possible to distinguish several prominent multimer peaks above the background signal (e.g.,

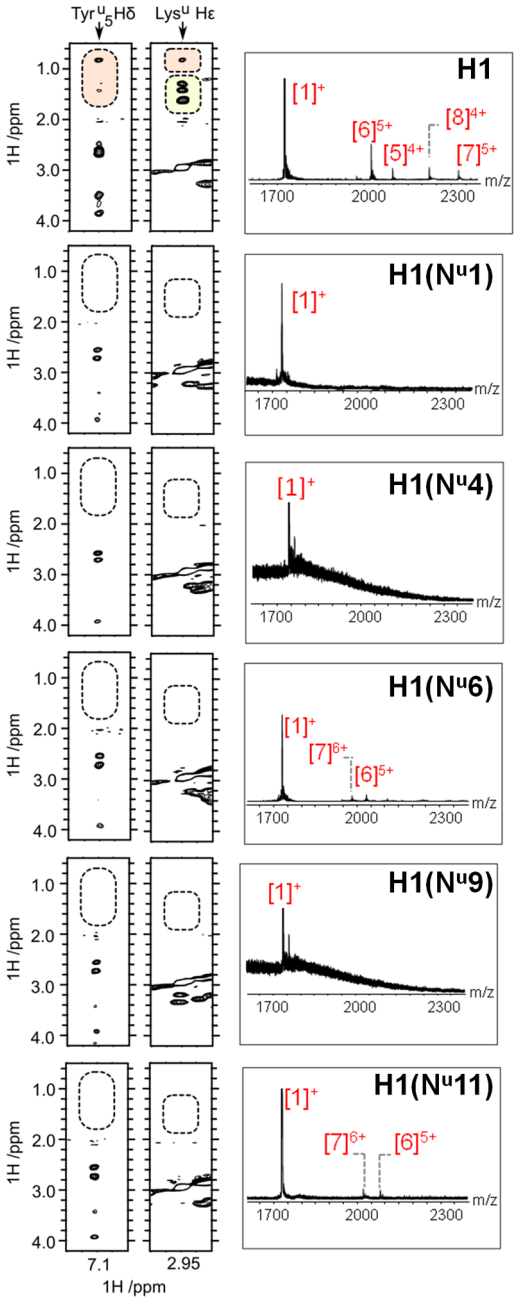

Figure 2. Selected parts of NOESY spectra and ESI-MS profiles of the N^u mutated series of **H1** analogues. **H1** is reported as a reference and measured under the same conditions. NMR 2D ^{1}H,^{1}H-NOESY spectra used a mixing time of 200 ms and were all measured as a 200 μM foldamer concentration in 20 mM sodium acetate (pH 4), 98% (v/v) D_2O, at 20 °C, with all spectra displayed at the same contour level. Dotted lines indicate regions that display characteristic NOE crosspeaks of the assembled bundles. Regions with a pale orange background signify the observation of inter-residue NOE crosspeaks to Y^u5 ^{1}H or K^u $^1H^\varepsilon$ nuclei, and pale yellow indicates intraresidue NOE crosspeaks to K^u $^1H^\varepsilon$ nuclei within ordered K^u side chains. A white background corresponds to an absence of these crosspeaks. A 100 μM solution in 20 mM ammonium acetate was used for the ESI-MS studies. The peak annotation $[n]^{z+}$ indicates the number of subunits n and the charge z of the detected assemblies.

DOI: 10.1021/jacs.6b05063
J. Am. Chem. Soc. 2016, 138, 10522−10530

2027.0 and 2084.1, corresponding to the $[7]^{6+}$ and $[6]^{5+}$ ions), suggesting that these oligoureas possess a slight tendency to self-assemble into discrete objects. These observations of nonspecific aggregates are consistent with the previously discussed NMR data for a population of the N^u-mutated oligoureas that transiently aggregates into highly dynamic assemblies. These ESI-MS data are also in line with the variable-concentration CD profiles measured for the N^u-mutated oligoureas, which indicate a degree of poorly defined aggregates (see Figure S2).

To investigate the thermal behavior of the N^u mutated analogues of **H1** and determine the stability of any higher-order assemblies, we performed variable-temperature CD experiments. The melting profiles of all five N^u mutants were reduced in intensity compared with **H1** (Figure 3), displaying a linear

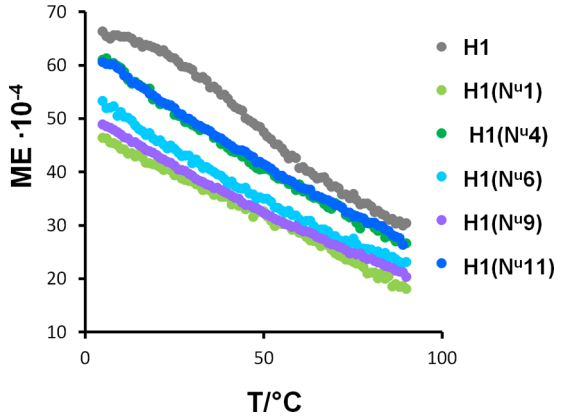

Figure 3. Variable-temperature CD experiments at 202 nm for all **H1** analogues containing the $L^u \rightarrow N^u$ replacement. Foldamers were analyzed at a concentration of 200 μM in 20 mM sodium acetate at pH 4. Molar ellipticity (ME) expressed in deg·cm^2 dmol^{-1}.

temperature dependence and noncooperative transition, again in contrast to the melting profile of **H1**. This behavior is consistent with the presence of minor higher-order (i.e., discrete self-assembled) species (**H1**(N^u**6**) and **H1**(N^u**11**)) or, alternatively, the presence of a highly dynamic or nondiscrete continuum of structures in aqueous conditions, again in good agreement with NMR and ESI-MS data.

It is therefore apparent that the insertion of a polar residue (N^u) within the hydrophobic surface of **H1** has a disruptive effect on bundle formation, regardless of the position (*a* or *d* positions of the oligourea helix) of the modification. This also suggests that a hydrophobic surface composed of five L^u residues is likely to be the minimum requirement for formation of a discrete bundle driven by specific hydrophobic packing interactions. Hence the creation of an oligourea helix bundle containing polar side chains pointing toward the hydrophobic interior would probably require the design of longer oligourea sequences with an increased number of hydrophobic side chains at the *a* and *d* positions, whose collective interactions would compensate for the introduction of otherwise destabilizing polar residues.[41] It remains to be seen whether the inclusion of polar residues in oligoureas could play the role of a negative design element to preferentially destabilize alternative structures over a target structure, similar to what is observed in peptide coiled-coil design.[37]

Modulation of the Hydrophobic Environment of the Cavity. The presence of an isolated cavity within the hydrophobic L^u-rich core of the **H1**-bundle represents a promising feature with respect to functionalization and future application of this foldamer system (Figure 1A), particularly with respect to guest encapsulation. According to the crystallographic data obtained previously,[32,33] the residues most directly involved in the formation of the cavity are L^u4, L^u6, and to a lesser extent L^u9, which pack to create a void space with a volume of 495.0 Å^3 (Figure 1A). In order to (1) understand the role of residues L^u4, L^u6, and L^u9 in the formation of the **H1**-bundle cavity and (2) modulate the size and shape of this cavity (as a step toward future application of the **H1**-bundle), we synthesized three analogues of **H1** containing individual hydrophobic modifications of the aforementioned L^u positions (L^u4, L^u6, and L^u9) with valine-type (V^u) residues (oligoureas **H1**(V^u**4**), **H1**(V^u**6**), and **H1**(V^u**9**)) (Figure 1B). In addition, we designed an additional **H1** analogue in which L^u6 was replaced with an isoleucine-type residue (I^u6) (oligourea **H1**(I^u**6**)), to gain insight into the possibility of fine-tuning the hydrophobic interactions and cavity shape.

CD analysis of oligoureas **H1**(V^u**6**), **H1**(V^u**9**), and **H1**(I^u**6**) indicated these foldamers to be helical in aqueous conditions, with variable-concentration experiments suggesting that these molecules self-assemble (Figure S2). (It should be noted that **H1**(V^u**4**) proved insoluble in water and thus could not be characterized. For further details, see SI.) NMR spectroscopy analysis of oligoureas **H1**(V^u**6**), **H1**(V^u**9**), and **H1**(I^u**6**) revealed NOE cross-peaks indicative of helix-bundle formation for all three molecules. In particular, the NOE cross-peaks between the aromatic Y^u5 protons and the aliphatic protons of L^u11 residues were observed, along with those between the CH_2 of the K^u side chains. This suggests that oligoureas **H1**(V^u**6**), **H1**(V^u**9**), and **H1**(I^u**6**) are involved in interactions that rigidify the overall structure, a finding that is compatible with the presence of stable quaternary arrangements. In addition, 1D ^{1}H NMR spectra of **H1**(V^u**6**), **H1**(V^u**9**), and **H1**(I^u**6**) revealed broad upfield-shifted methyl ^{1}H peaks (akin to **H1**), indicative of the existence of assembled multimeric objects in solution (Figure S3). ESI-MS analysis of **H1**(V^u**6**), **H1**(V^u**9**), and **H1**(I^u**6**) (in ammonium acetate) supported these findings, since it was possible to observe prevalent multimer peaks corresponding to the ion $[6]^{5+}$ within spectra collected for all three foldamers (Figure 4). These experiments all suggest that the **H1**(V^u**6**), **H1**(V^u**9**), and **H1**(I^u**6**) analogues of **H1** maintain a discrete hexameric assembly in aqueous conditions, implying that the interlocked hydrophobic packing and overall architecture is preserved when the L^u residues at positions 4, 6, or 9 are replaced by alternative nonpolar side chains (i.e., V^u and I^u).

CD-monitored thermal melting experiments showed that oligoureas **H1**(V^u**6**) and **H1**(V^u**9**) displayed melting profiles and cooperative unfolding similar to **H1** (Figure 5), with a concomitant high level of similarity in melting points for all three oligoureas (T_m values in buffered conditions for **H1**, **H1**(V^u**6**), and **H1**(V^u**9**) derived by fitting the data to a two-state unfolding transition are 48.9, 48.3, and 49.5 °C, respectively). Oligourea **H1**(I^u**6**), however, displayed a dramatically different CD-monitored melting profile, with a considerably reduced intensity compared with oligoureas **H1**, **H1**(V^u**6**), and **H1**(V^u**9**) (see also Figure S5 and Supporting Information) and no clear melting transition (a T_m value for **H1**(I^u**6**) can therefore not be determined). This suggests that, despite sharing an overall hexameric assembly, there are

DOI: 10.1021/jacs.6b05063
J. Am. Chem. Soc. 2016, 138, 10522−10530

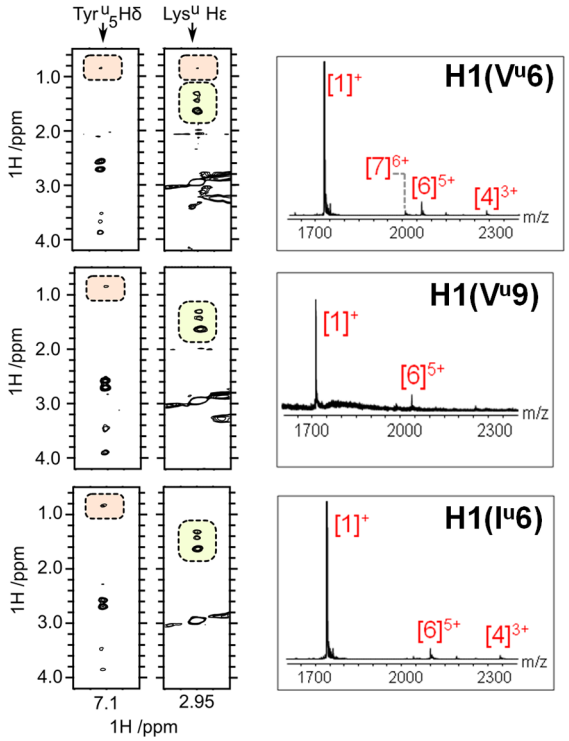

Figure 4. NOESY spectra and ESI-MS profiles of mutants of **H1** in which L^u at positions 6 and 9 are mutated to hydrophobic V^u or I^u residues. Data were collected and are presented as in Figure 2.

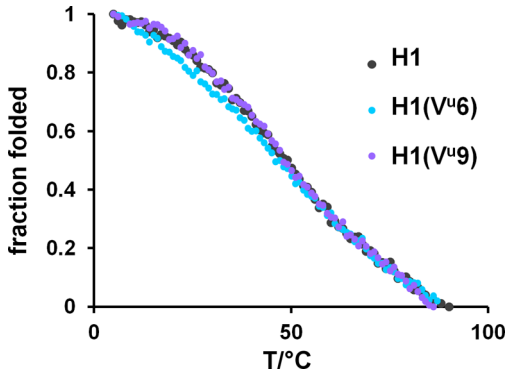

Figure 5. Variable-temperature CD experiments at 202 nm for **H1** analogues with L^u → V^u mutations at positions 6 or 9. The results are shown as fraction folded. Foldamers were analyzed at a concentration of 200 μM in 20 mM aqueous sodium acetate at pH 4.0. Note that previously reported CD-monitored thermal melting data for **H1** were for experiments performed in pure water.[32]

substantial differences in thermal stability of **H1(I^{u}6)** compared with oligoureas **H1**, **H1(V^{u}6)**, and **H1(V^{u}9)**.

In order to determine whether alterations in the volume of the void-space of the internal cavity could account for the differences observed in the thermal behavior of these molecules, we built theoretical models of **H1(V^{u}4)**, **H1(V^{u}6)**, and **H1(V^{u}9)** to calculate the cavity volumes of each mutant. The results obtained suggest that mutations in positions 4 and 6 have a greater impact on the volume of the cavity compared with modifications of position 9, with estimated cavity volumes of 611.9, 617.8, and 499 Å^3 for **H1(V^{u}4)**, **H1(V^{u}6)**, and **H1(V^{u}9)**, respectively (note, volume of the **H1**-bundle cavity is 495.0 Å^3) (Table S1). These findings are partially in line with CD-monitored thermal melting data, because **H1(V^{u}9)** and **H1** share similar cavity volumes and T_m values. However, it is perhaps surprising that **H1(V^{u}6)** possesses a T_m comparable with **H1**, despite the considerable increase in the cavity volume of **H1(V^{u}6)**. This suggests that either (1) the cavity is amenable to significant increases in internal capacity or (2) CD experiments, representing a weighted average property of all the oligomeric states in solution, do not accurately characterize the hexamer fraction. Because NMR and ESI-MS findings suggest that **H1(V^{u}6)** is able to self-assemble into discrete objects in aqueous conditions, it is likely that the self-assembled helix bundle arrangement is indeed compatible with large increases in cavity volume. This finding has implications with respect to the nature of the guest molecules that could be encapsulated by **H1**-related bundles.

A theoretical cavity volume was also calculated for oligourea **H1(I^{u}6)**, revealing a void volume similar to that of the **H1**-bundle (434.8 Å^3). This perhaps unsurprising similarity in cavity volume does not account for the deviant melting profile determined for **H1(I^{u}6)** from CD-monitored melting experiments, although it is possible that the modest reduction in cavity volume observed for **H1(I^{u}6)** (compared with **H1**) is responsible for such CD-based effects. Nevertheless, both NMR and ESI-MS have provided evidence of the formation of discrete assemblies of **H1(I^{u}6)** in solution. As seen for **H1(V^{u}6)**, it is likely that L^u → I^u modifications of the hydrophobic core of **H1** are also compatible with helical bundle formation.

On the Role of the Terminal L^u Residues of the H1-Bundle: Interplay of Primary, Secondary, and Quaternary Structure. While it is clear that, based on solution and high resolution structural data, the three central Leu^u residues of **H1** (L^{u}4, L^{u}6, and L^{u}9) play a key role in bundle formation through the formation of precise KIH-type packing interactions, the role of the remaining two terminal Leu^u residues, L^{u}1 and L^{u}11, is less obvious. The leucine-type isobutyl side chains of both of these residues within the **H1**-bundle are orientated toward the central hydrophobic cavity based on the crystal structure.[32] However, it seems that these residues play a less significant role in bundle formation than the central L^u residues, and there is evidence that neither of these residues is optimally positioned. For example, the intrahelical hydrogen bonds involving L^{u}1 (terminal carbonyl group) of the **H1**-bundle are noticeably longer than the average intrahelical hydrogen bond length (by up to 0.5 Å, for chain A), with several of the backbone torsion angles of L^{u}11 deviating significantly from those of a canonical oligourea helix. Both of these observations suggest suboptimal side chain packing, and as such, we wanted to investigate the role of these terminal residues in bundle formation at the atomic level, with a view to (1) potentially improve bundle robustness and (2) functionally modify the bundle for eventual applications.

While NMR studies indicated that replacement of residues L^{u}1 and L^{u}11 with N^u resulted in a loss in detectable helix bundle formation, the same experiments for **H1** analogues bearing valine-type urea residues at either of these terminal positions, **H1(V^{u}1)** and **H1(V^{u}11)** (synthesized as described above), indicated bundle formation to be compatible with these hydrophobic replacements (Figure 6). These results were supported by ESI-MS studies (Figure 6), which showed the predominant multimer formed by **H1(V^{u}1)** and **H1(V^{u}11)** (albeit to a lesser extent) to be hexameric.

In order to investigate the effects of these terminal hydrophobic modifications on the secondary and quaternary

DOI: 10.1021/jacs.6b05063
J. Am. Chem. Soc. 2016, 138, 10522−10530

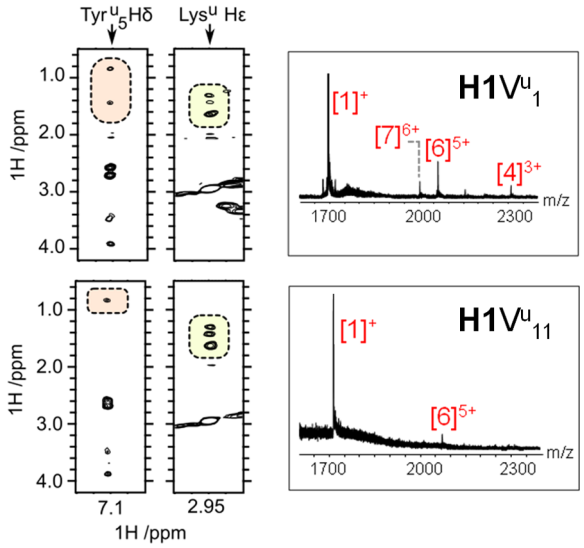

Figure 6. NOESY spectra and ESI-MS profiles of mutants of **H1** in which L^u residues at the terminal positions 1 and 11 are mutated to a hydrophobic V^u residue. Data were collected and are presented as in Figure 2.

structural features at the atomic level, crystal structures of **H1(V^{u}1)** and **H1(V^{u}11)** were determined, with resolutions of 1.44 and 1.50 Å, respectively (Tables 1 and S2). Crystals were

Table 1. Summary of H1-Analogue Crystal Structures Reported in This Work[a]

	structure 1	structure 2	structure 3	structure 4
oligourea	**H1(V^{u}1)**	**H1(V^{u}11)**	**H1(V^{u}1)**	**H1(V^{u}11)**
space group	$P6_3$	$P6_3$	$C2$	$P2_12_12$
resolution (Å)	1.44	1.50	0.97	0.94
R_{work} (%)	18.52	23.23	12.22	13.15
R_{free} (%)	23.28	28.82	13.25	15.05
CCDC code	1415873	1415874	1415872	1415875

[a]Full crystallographic data collection and refinement details can be found in Table S2.

grown from conditions comparable to those from which **H1** crystallized,[32] and indeed the crystals of both **H1(V^{u}1)** and **H1(V^{u}11)** yielded hexameric helix bundle structures isomorphous with the **H1**-bundle previously reported (referred to as structures 1 and 2, for **H1(V^{u}1)** and **H1(V^{u}11)**, respectively) (see Tables 1, S2, and S3, Figure 7A,B, and Figure S6). Globally, the discrete helix bundle quaternary arrangements formed by **H1**, **H1(V^{u}1)**, and **H1(V^{u}11)** in the crystal state are all highly similar with RMSDs of 0.339 and 0.654 Å for **H1** vs **H1(V^{u}1)** and **H1(V^{u}11)**, respectively (see Table S3 and Figure S6); however, there are subtle differences in backbone and side chain geometry among these three analogues, which have a significant impact on the interhelical packing interactions of the helix bundle.

In the crystal structure, replacement of the L^{u}1 residue of **H1** with V^u results in improved helix geometry (Figure 7A,C), as measured by a shortening of the two intrahelical NH···CO hydrogen bonds at the N terminal extremity, from 3.6 and 3.4 Å (of **H1**, chain A) to 3.5 and 2.8 Å (**H1(V^{u}1)**, chain A), and from 3.2 and 3.1 Å (**H1**, chain B) to 3.1 and 3.0 Å (**H1(V^{u}1)**, chain B). Analysis of the **H1** crystal structure indicates that the leucine-type side chain of the first residue of this oligourea is

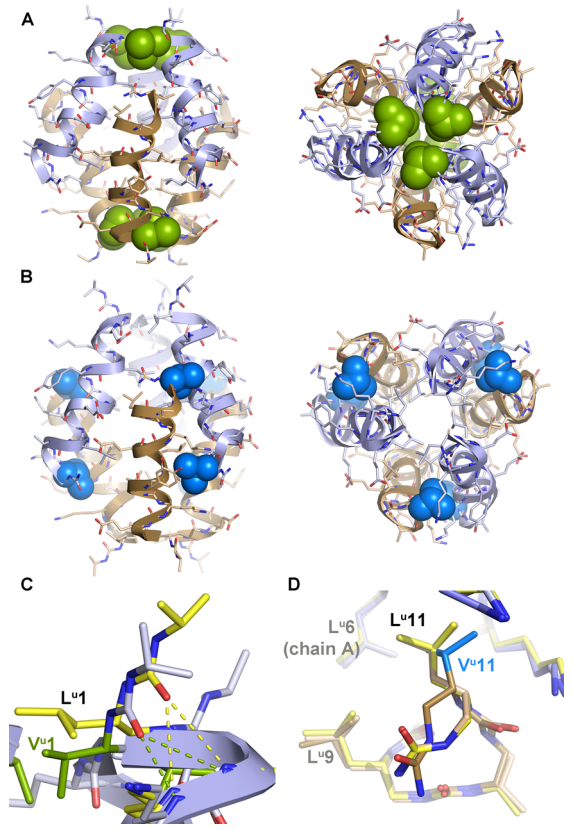

Figure 7. Crystal structures of helix bundles formed from **H1** analogues, **H1(V^{u}1)**, structure 1 (A), and **H1(V^{u}11)**, structure 2 (B), and comparison with **H1** helix bundle crystal structure (C, D). (C) Detail of the H-bond network surrounding the first residue in **H1** and **H1(V^{u}1)** (chain A). (D) Overlay of chains B of **H1**, **H1(V^{u}1)**, and **H1(V^{u}11)** reveals a distortion of the helix termination in **H1(V^{u}11)**. In both structures 1 and 2, carbon atoms of chain A are shown in light-blue whereas those of chain B are colored wheat. Carbon atoms of **H1** are shown in yellow. The V^u side chains are colored according to their position in the sequence, using the color code of Figure 1.

too large to be accommodated favorably in the bundle arrangement, resulting in steric clashes with the N terminal regions of neighboring helices and causing the helix to bend away from the hydrophobic core. Reduction of the length of this side chain by one carbon (in the case **H1(V^{u}1)**, structure 1) appears to alleviate this apparent steric clash, allowing the foldamer to adopt a more canonical, less bent (and presumably more stable) helical geometry within the bundle arrangement (Figure 7A,C) in agreement also with ESI-MS studies (Figure 6).

In contrast to modification of L^{u}1, the crystal structure of **H1(V^{u}11)** (structure 2) shows that replacement of the **L^{u}11** residue of **H1** with V^u reduces the helicity at the C-terminus of chain A (for chain B, see below), as measured by intrahelical NH···CO hydrogen bond distances. The shortening of the Leu-type side chain of residue 11 by one carbon atom compromises an important interhelical packing contact of the helix bundle (primarily involving the L^{u}6 side chain of a neighboring helix), causing the C termini of the **H1(V^{u}11)** helices to distort in order to maintain this packing interaction. Although this loss of helicity at the C termini would be expected to result in a reduction in bundle stability, it appears that the helices of the bundle can nevertheless adapt in order to compensate for this L^u → V^u modification (Figure 7B). Further structural evidence

DOI: 10.1021/jacs.6b05063
J. Am. Chem. Soc. 2016, 138, 10522−10530

of the ability of the **H1(V^{u}11)** helices to adapt in order to maintain the bundle arrangement can be seen when examining the second chain (chain B) of the asymmetric unit, which reveals the backbone of the C terminal V^{u}11 residue to be considerably restructured compared with the equivalent residues of **H1**, as well as compared with chain A of **H1(V^{u}11)** (Table S4 and Figure 7D). This backbone rearrangement permits the retention of key interhelical packing interactions (involving L^{u}6 side chains of neighboring helices), as well as intrahelical hydrogen bonds.

Overall, these two crystal structures (structures 1 and 2) suggest that replacement of L^{u}1 with V^u could potentially improve the overall stability of the helix bundle (compared with the **H1**-bundle), while replacement of L^{u}11 with V^u could have the opposite effect. To what degree are these structural findings supported by solution data? Both NMR and ESI-MS analyses of **H1(V^{u}1)** and **H1(V^{u}11)** (Figure 6) provide semiquantitative evidence that **H1(V^{u}1)** is indeed more prone to self-assemble than **H1(V^{u}11)**, suggestive of improved bundle stability in the case of **H1(V^{u}1)**, and therefore in reasonable agreement with the crystallographic data. However, definitive quantitative correlation between the crystal structures of **H1**, **H1(V^{u}1)**, and **H1(V^{u}11)** and the solution behavior of these compounds is not absolute, perhaps because the structural differences among these three analogous helix bundles are too subtle to have a significant impact on overall bundle stability. Indeed, the similarity in the solution behavior of **H1**, **H1(V^{u}1)**, and **H1(V^{u}11)** is highlighted by the rather narrow range into which CD-monitored T_m values for these foldamers fall (see Figure 8).

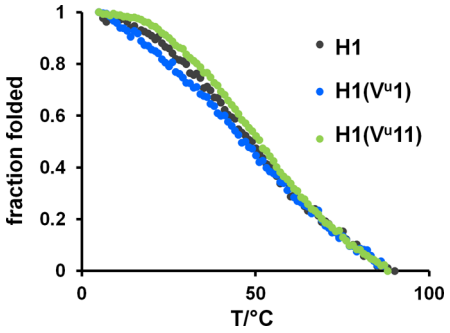

Figure 8. Variable-temperature CD experiments at 202 nm for **H1** analogues containing hydrophobic mutations (L^u → V^u) at terminal positions. The results are shown as fraction folded. Foldamers were analyzed at a concentration of 200 μM in 20 mM aqueous sodium acetate at pH 4.0. Equivalent ME data are shown in Figure S5 and yield T_m values (in °C) of 48.9, 46.0, and 51.2 for **H1**, **H1(V^{u}1)**, and **H1(V^{u}11)**, respectively.

The crystallographic data suggests that the progenitor helix (**H1**) together with the **H1(V^{u}1)** and **H1(V^{u}11)** analogues, and most likely amphiphilic water-soluble oligourea helices in general, possess an intrinsic degree of structural flexibility, enabling the secondary structures of these foldamers to adapt in order to form quaternary packing interactions. This proposition is supported further by the determination of alternative high resolution crystal forms of both **H1(V^{u}1)** and **H1(V^{u}11)** in conditions that destabilize the hexamer (Tables 1 and S2). The **H1** and **H1**-type helix bundles require acidic conditions in order to form, because charge clashes involving the Glu-type side chains (particularly involving E^{u}7 residues) are expected to occur at a pH above the carboxylate pK_a (i.e., at pH values >4.5). Consequently, the structures determined for **H1(V^{u}1)** and **H1(V^{u}11)** for crystals grown in mildly basic conditions (structures 3 and 4, Figure 9A,B) reveal a loss of (discrete)

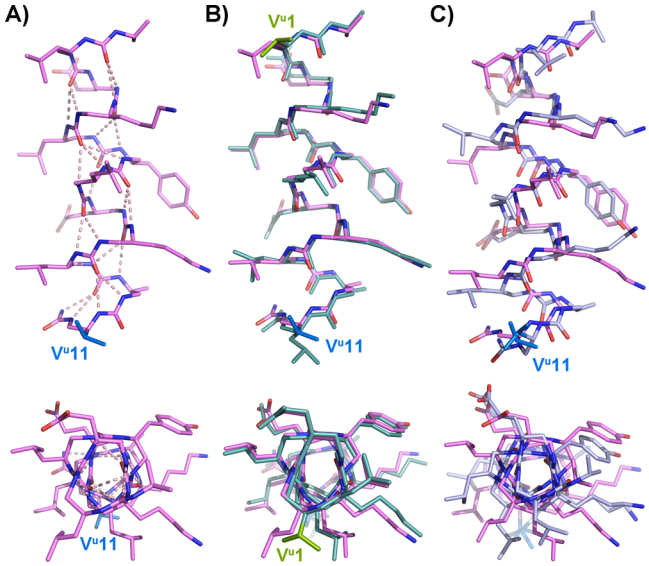

Figure 9. Structures of nonassembled **H1(V^{u}1)** (structure 3) and **H1(V^{u}11)** (structure 4) helices from crystals grown in mildly basic conditions. (A) Structure 4 alone. (B) Overlay of structures 3 (carbon atoms are shown in light teal) and 4 (carbon atoms are shown in violet). The RMSD for this alignment is 0.748 Å (95 to 95 atoms). (C) Overlay of the structures of **H1(V^{u}11)** in assembled (structure 2, chain A, carbon atoms of chain A are colored as in Figure 7) and nonassembled state (structure 4). The RMSD for this alignment is 2.113 Å (121 to 121 atoms). The V^u side chains are colored according to their position in the sequence, using the color code of Figure 1.

quaternary assembly for structures 3 and 4. The asymmetric units contain just one helix, with the low symmetry of the space groups revealing no discernible quaternary structure. The structures of **H1(V^{u}1)** and **H1(V^{u}11)** for crystals grown from basic conditions (structures 3 and 4) can thus be considered as isolated helices. The ultrahigh resolution of the data (0.97 and 0.94 Å for **H1(V^{u}1)** and **H1(V^{u}11)**, respectively) provides a valuable opportunity to compare the changes in secondary structures between the assembled and nonassembled states. Indeed, striking differences in secondary structure between the monomers and hexameric assemblies are apparent, crudely evidenced by the high RMSD values generated from structural alignments — 1.877/1.949 Å for structure 3 vs structure 1 (chains A/B), and 2.113/2.089 Å for structure 4 vs structure 2 (chains A/B) (see Figure 9C and Table S3).

In contrast, the nonassembled structures (structures 3 and 4) are remarkably similar to each other, with an RMSD value of just 0.748 Å (Figure 9B and Table S3). Comparison of average helical parameter values (Table 2) provides an explanation for such dramatic differences in the three-dimensional structures of the assembled and nonassembled foldamers. In the absence of higher order assembly, it appears that the helical geometries of the monomeric **H1(V^{u}1)** and **H1(V^{u}11)** (structures 3 and 4) adhere strictly to canonical oligourea helix parameters.[33,42] However, upon hexamer formation these same foldamers display structural plasticity in order to support quaternary arrangements (structures 1 and 2), as evidenced by significant deviations in average Cα torsion angles and helix bending

DOI: 10.1021/jacs.6b05063
J. Am. Chem. Soc. 2016, 138, 10522−10530

Table 2. Average Helical Parameters of Oligoureas H1 and H1-Analogue Crystal Structures[a]

crystal structure	residue/turn	rise (Å)	rise/turn (Å)	radius (Å)	twist/residue (deg)	Cα torsion[b] (deg)	mean bending angle[c] (deg)
H1(V^{u}1) *C*2	2.52	2.02	5.05	2.82	142.79	93.88	4.29
H1(V^{u}1) $P6_3$ (chain A)	2.47	2.07	5.11	2.75	145.48	99.71	14.72
H1(V^{u}1) $P6_3$ (chain B)	2.48	2.06	5.11	2.76	145.44	99.79	14.30
H1(V^{u}11) $P2_12_12$	2.55	1.95	4.97	2.83	141.16	90.28	6.26
H1(V^{u}11) $P6_3$ (chain A)	2.48	2.09	5.18	2.75	145.07	99.63	13.56
H1(V^{u}11) $P6_3$ (chain B)	2.47	2.07	5.11	2.73	145.66	100.47	9.73
H1 (chain A)[32]	2.47	2.09	5.16	2.74	146.02	101.23	15.66
H1 (chain B)[32]	2.47	2.11	5.21	2.75	145.80	101.06	15.25

[a]Analysis performed using the HELANAL-Plus server.[43] [b]Average virtual torsion angle defined by four consecutive Cα atoms. [c]Average bending angle between successive local helix axes.

angles (helical parameter values and definitions are provided in Table 2). The individual helices of the **H1(V^{u}1)** bundle, for example, are bent on average by over 14°, approximately 10° greater than the nonassembled oligourea helix. The advantageous ability to study both the monomeric and hexameric forms of the same oligoureas illustrates that packing interactions have a significant impact on their secondary structures and demonstrates that water-soluble oligoureas possess an unpredicted and significant degree of structural plasticity.

CONCLUSIONS

Oligoureas represent a unique helical platform for the fabrication of nanostructures in aqueous conditions, yet the principles that govern their folding and self-assembly remain to be fully described. By using an oligourea foldamer previously shown to self-assemble into a discrete helix bundle and systematically replacing each leucine-type residue with hydrophilic asparagine-type residues (N^u), we see that any disruption of the hydrophobic helix seam prevents detectable self-assembly. Based on the high-resolution crystal structure of the **H1**-bundle,[32,33] the majority of the Leu-type side chains (L^u) take part in key KIH-type packing interactions, thus the replacement of these residues with nonhydrophobic moieties might be expected to disrupt helix-bundle formation. However, hydrophilic residues are frequently located within the hydrophobic regions of α-peptides involved in helix−helix contacts within helix bundles,[37,38,44] thus the **H1**-Asn^u mutants described above could feasibly have been compatible with helix-bundle formation. Why do these Asn^u replacements of **H1** appear to have such a dramatic (and negative) effect on helix-bundle formation? It is possible that the short length of these oligourea helices (compared with typical helix-bundle forming α-peptides[41]) is responsible for this behavior and that significantly longer amphiphilic oligoureas may tolerate the insertion of hydrophilic residues within hydrophobic regions. Future development of functional oligourea assemblies (such as in substrate binding or ion transport) could therefore include longer component helices. The isolated cavity located within the hydrophobic core of the **H1**-bundle represents a particularly attractive motif for future application of this (and related) foldamer(s). This isolated cavity is enclosed almost entirely by Leu-type side chains, several of which we have shown here can be modified to alternative side chains while maintaining bundle integrity. These theoretical and experimental findings suggest that the size and shape of this cavity could feasibly be engineered in the future, which has enticing implications with respect to future application.

High-resolution structural insight into the formation of the **H1**-bundle has also been provided here, with crystal structures of two terminal Leu^u → Val^u mutants confirming the formation of six-helix bundles for these foldamers, as well as uncovering subtle yet potentially meaningful structural variations between these assemblies and the parent **H1**-assembly. In addition, the determination of additional crystal forms of each of these **H1** analogues provides an interesting structural view of the effect of the quaternary assembly on secondary structure. These additional crystal forms, both ultrahigh resolution, could be considered to represent nonassembled structural forms of these foldamers and indicate that the helical geometry of each foldamer remodels significantly as a consequence of quaternary (bundle) packing. This apparent structural plasticity of these amphiphilic oligoureas could partially hamper efforts to rationally design new and improved aqueous assemblies, since these effects are currently difficult to predict. However, the ability of the **H1(V^{u}1)** and **H1(V^{u}11)** foldamers to structurally adapt to quaternary packing arrangements (observed crystallographically) suggests that the foldamers themselves may be able to compensate for imperfect sequence design.

Considering the relatively limited number of reports describing precise quaternary assemblies built from non-natural polymers, it is not surprising that the rules governing the folding and assembly of amphiphilic foldamers in aqueous conditions are less well understood than those governing polypeptide folding. Yet progress toward understanding foldamer self-assembly is underway and will be necessary for the controlled and directed construction of precise, functional, non-natural entities in aqueous conditions. The findings we have reported here outline several key requirements for helix bundle formation by an amphiphilic oligourea. This information, coupled with automated synthesis of oligoureas for sequence diversity, will be exploited to (1) improve the current stability of the six-helix foldamer bundle described previously; (2) engineer functional properties into oligourea aqueous assemblies, and (3) expand the range of bundle topologies by modulating interhelix arrangements.

ASSOCIATED CONTENT

Supporting Information

Crystallographic data for **H1(V^{u}1)** (structures 1 and 3) and **H1(V^{u}11)** (structures 2 and 4) (CIF). The Supporting Information is available free of charge on the ACS Publications website at DOI: 10.1021/jacs.6b05063.

Experimental procedures and characterization data, supplemental Figures S1−S6, Tables S1−S5 and supplemental references (PDF)

Crystallographic data for **H1(V^{u}1)**, structure 3 (CIF)

DOI: 10.1021/jacs.6b05063
J. Am. Chem. Soc. 2016, 138, 10522−10530

Crystallographic data for **H1(V^{u}1)**, structure 3 (PDB)
Crystallographic data for **H1(V^{u}1)**, structure 1 (CIF)
Crystallographic data for **H1(V^{u}1)**, structure 1 (PDB)
Crystallographic data for **H1(V^{u}11)**, structure 2 (CIF)
Crystallographic data for **H1(V^{u}11)**, structure 2 (PDB)
Crystallographic data for **H1(V^{u}11)**, structure 4 (CIF)
Crystallographic data for **H1(V^{u}11)**, structure 4(PDB)

AUTHOR INFORMATION

Corresponding Author

*g.guichard@iecb.u-bordeaux.fr

Present Addresses

[¶]G.W.C.: Division of Cancer Therapeutics, Institute of Cancer Research, 15 Cotswold Road, Sutton, London, SM2 5NG, United Kingdom.
[○]K.P.-Z.: Faculty of Chemistry, University of Warsaw, Pasteura 1, 02-093 Warsaw, Poland.

Author Contributions

[▽]C.M.L. and G.W.C. contributed equally to the work.

Notes

The authors declare no competing financial interest.

ACKNOWLEDGMENTS

This work was supported by the CNRS, Conseil Régional d'Aquitaine (Project No. 20091102003 and ANR (Project No. ANR-12-BS07-0019)). Marie Curie FP7-PEOPLE-2010-IEF-273224 and FP7-PEOPLE-2012-IEF-330825 postdoctoral fellowships (to K.P.-Z. and C.M.L.) are gratefully acknowledged. We are grateful to the European Synchrotron Radiation Facility and SOLEIL synchrotron for providing access to X-ray facilities and to Pierre Legrand for assistance on beamline PROXIMA 1.

REFERENCES

(1) Burkhard, P.; Stetefeld, J.; Strelkov, S. V. *Trends Cell Biol.* **2001**, *11*, 82−88.
(2) Bromley, E. H. C.; Channon, K.; Moutevelis, E.; Woolfson, D. N. *ACS Chem. Biol.* **2008**, *3*, 38−50.
(3) Robson Marsden, H.; Kros, A. *Angew. Chem., Int. Ed.* **2010**, *49*, 2988−3005.
(4) Lupas, A. N.; Gruber, M. In *Advances in Protein Chemistry*; Richards, F. M., Eisendberg, D. S., Parry, D. A. D., Squire, J. M., Eds.; Academic Press: Boston, MA, 2005; Vol. *70*, pp 37−38.
(5) Woolfson, D. N.; David, A. D. P.; John, M. S. In *Advances in Protein Chemistry*; Richards, F. M., Eisendberg, D. S., Parry, D. A. D., Squire, J. M., Eds.; Academic Press: Boston, MA, 2005; Vol. *70*, pp 79−112.
(6) Moutevelis, E.; Woolfson, D. N. *J. Mol. Biol.* **2009**, *385*, 726−732.
(7) Apostolovic, B.; Klok, H.-A. *Biomacromolecules* **2008**, *9*, 3173−3180.
(8) Schnarr, N. A.; Kennan, A. J. *Org. Lett.* **2005**, *7*, 395−398.
(9) Betz, S. F.; Bryson, J. W.; DeGrado, W. F. *Curr. Opin. Struct. Biol.* **1995**, *5*, 457−463.
(10) Horne, W. S.; Yadav, M. K.; Stout, C. D.; Ghadiri, M. R. *J. Am. Chem. Soc.* **2004**, *126*, 15366−15367.
(11) Liu, J.; Zheng, Q.; Deng, Y.; Cheng, C.-S.; Kallenbach, N. R.; Lu, M. *Proc. Natl. Acad. Sci. U. S. A.* **2006**, *103*, 15457−15462.
(12) Zaccai, N. R.; Chi, B.; Thomson, A. R.; Boyle, A. L.; Bartlett, G. J.; Bruning, M.; Linden, N.; Sessions, R. B.; Booth, P. J.; Brady, R. L.; Woolfson, D. N. *Nat. Chem. Biol.* **2011**, *7*, 935−941.
(13) Thomson, A. R.; Wood, C. W.; Burton, A. J.; Bartlett, G. J.; Sessions, R. B.; Brady, R. L.; Woolfson, D. N. *Science* **2014**, *346*, 485−488.
(14) Dong, H.; Paramonov, S. E.; Hartgerink, J. D. *J. Am. Chem. Soc.* **2008**, *130*, 13691−13695.
(15) Xu, C.; Liu, R.; Mehta, A. K.; Guerrero-Ferreira, R. C.; Wright, E. R.; Dunin-Horkawicz, S.; Morris, K.; Serpell, L. C.; Zuo, X.; Wall, J. S.; Conticello, V. P. *J. Am. Chem. Soc.* **2013**, *135*, 15565−15578.
(16) Fletcher, J. M.; Harniman, R. L.; Barnes, F. R. H.; Boyle, A. L.; Collins, A.; Mantell, J.; Sharp, T. H.; Antognozzi, M.; Booth, P. J.; Linden, N.; Miles, M. J.; Sessions, R. B.; Verkade, P.; Woolfson, D. N. *Science* **2013**, *340*, 595−599.
(17) Gradišar, H.; Božič, S.; Doles, T.; Vengust, D.; Hafner-Bratkovič, I.; Mertelj, A.; Webb, B.; Šali, A.; Klavžar, S.; Jerala, R. *Nat. Chem. Biol.* **2013**, *9*, 362−366.
(18) Thomas, F.; Burgess, N. C.; Thomson, A. R.; Woolfson, D. N. *Angew. Chem., Int. Ed.* **2016**, *55*, 987−991.
(19) Apostolovic, B.; Danial, M.; Klok, H.-A. *Chem. Soc. Rev.* **2010**, *39*, 3541−3575.
(20) Gellman, S. H. *Acc. Chem. Res.* **1998**, *31*, 173−180.
(21) Guichard, G.; Huc, I. *Chem. Commun.* **2011**, *47*, 5933−5941.
(22) Goodman, C. M.; Choi, S.; Shandler, S.; DeGrado, W. F. *Nat. Chem. Biol.* **2007**, *3*, 252−262.
(23) Horne, W. S. *Nat. Chem.* **2015**, *7*, 858−859.
(24) Gopalan, R. D.; Del Borgo, M. P.; Mechler, A. I.; Perlmutter, P.; Aguilar, M.-I. *Chem. Biol.* **2015**, *22*, 1417−1423.
(25) Pavone, V.; Zhang, S.-Q.; Merlino, A.; Lombardi, A.; Wu, Y.; DeGrado, W. F. *Nat. Commun.* **2014**, *5*, 3581.
(26) Daniels, D. S.; Petersson, E. J.; Qiu, J. X.; Schepartz, A. *J. Am. Chem. Soc.* **2007**, *129*, 1532−1533.
(27) Goodman, J. L.; Petersson, E. J.; Daniels, D. S.; Qiu, J. X.; Schepartz, A. *J. Am. Chem. Soc.* **2007**, *129*, 14746−14751.
(28) Molski, M. A.; Goodman, J. L.; Chou, F.-C.; Baker, D.; Das, R.; Schepartz, A. *Chem. Sci.* **2013**, *4*, 319−324.
(29) Horne, W. S.; Price, J. L.; Keck, J. L.; Gellman, S. H. *J. Am. Chem. Soc.* **2007**, *129*, 4178−4180.
(30) Giuliano, M. W.; Horne, W. S.; Gellman, S. H. *J. Am. Chem. Soc.* **2009**, *131*, 9860−9861.
(31) Horne, W. S.; Price, J. L.; Gellman, S. H. *Proc. Natl. Acad. Sci. U. S. A.* **2008**, *105*, 9151−9156.
(32) Collie, G. W.; Pulka-Ziach, K.; Lombardo, C. M.; Fremaux, J.; Rosu, F.; Decossas, M.; Mauran, L.; Lambert, O.; Gabelica, V.; Mackereth, C. D.; Guichard, G. *Nat. Chem.* **2015**, *7*, 871−878.
(33) Collie, G. W.; Pulka-Ziach, K.; Guichard, G. *Chem. Commun.* **2016**, *52*, 1202−1205.
(34) Kwon, S.; Kim, B. J.; Lim, H.-K.; Kang, K.; Yoo, S. H.; Gong, J.; Yoon, E.; Lee, J.; Choi, I. S.; Kim, H.; Lee, H.-S. *Nat. Commun.* **2015**, *6*, 8747.
(35) Chothia, C.; Levitt, M.; Richardson, D. *J. Mol. Biol.* **1981**, *145*, 215−250.
(36) O'Shea, E.; Klemm, J.; Kim, P.; Alber, T. *Science* **1991**, *254*, 539−544.
(37) Gonzalez, L.; Woolfson, D. N.; Alber, T. *Nat. Struct. Biol.* **1996**, *3*, 1011−1018.
(38) Akey, D. L.; Malashkevich, V. N.; Kim, P. S. *Biochemistry* **2001**, *40*, 6352−6360.
(39) Douat-Casassus, C.; Pulka, K.; Claudon, P.; Guichard, G. *Org. Lett.* **2012**, *14*, 3130−3133.
(40) Douat, C.; Aisenbrey, C.; Antunes, S.; Decossas, M.; Lambert, O.; Bechinger, B.; Kichler, A.; Guichard, G. *Angew. Chem., Int. Ed.* **2015**, *54*, 11133−11137.
(41) Su, J. Y.; Hodges, R. S.; Kay, C. M. *Biochemistry* **1994**, *33*, 15501−15510.
(42) Fischer, L.; Claudon, P.; Pendem, N.; Miclet, E.; Didierjean, C.; Ennifar, E.; Guichard, G. *Angew. Chem., Int. Ed.* **2010**, *49*, 1067−1070.
(43) Kumar, P.; Bansal, M. *J. Biomol. Struct. Dyn.* **2012**, *30*, 773−783.
(44) Oakley, M. G.; Kim, P. S. *Biochemistry* **1998**, *37*, 12603−12610.

DOI: 10.1021/jacs.6b05063
J. Am. Chem. Soc. 2016, 138, 10522−10530